HHS Public Access

Author manuscript

J Control Release. Author manuscript; available in PMC 2020 December 10.

Published in final edited form as:

J Control Release. 2019 December 10; 315: 40–54. doi:10.1016/j.jconrel.2019.10.039.

A cerium oxide loaded glycol chitosan nano-system for the treatment of dry eye disease

Fan Yu[a,b], **Min Zheng**[b], **Alice Yang Zhang**[b], **Zongchao Han**[b,c,*]

[a]Jiangsu Provincial Key Laboratory of Coastal Wetland Bioresources, School of pharmacy, Yancheng Teachers University, Yancheng City, Jiangsu Province, P.R.China

[b]Department of Ophthalmology, the University of North Carolina at Chapel Hill, Chapel Hill, North Carolina 27599, USA

[c]Division of Pharmacoengineering & Molecular Pharmaceutics, Eshelman School of Pharmacy, the University of North Carolina at Chapel Hill, Chapel Hill, North Carolina 27599, USA

Abstract

Dry eye (DE) disease is an uprising health epidemic that directly affects the surface of the eye. We developed a water soluble cerium oxide loaded glycol chitosan nanoparticle as a new type of eye drop, namely GCCNP (glycol chitosan cerium oxide nanoparticles). GCCNP is capable of scavenging cellular reactive oxygen species (ROS) for the treatment of DE disease. The antioxidative effects of GCCNP were assessed in mice primary corneal and conjunctival cells *in vitro* and in a DE murine model *in vivo*. GCCNP's effect on the DE models was assessed via histological evaluations, migration assays, cell viability assays, cellular uptake analyses, intracellular ROS scavenging assays, wound healing assays, mitochondrial membrane potential readings, corneal fluorescein staining, tear volume concentrations, tear film break up time analyses, and lastly, analytical/spectroscopic analyses of GCCNP eye drop formulations. Spectroscopic analysis showed that cerium oxide was entrapped into the glycol chitosan (GC). The solubility of cerium in GC (GCCNP) increased to 709.854±24.3 μg/ml compared to its original solubility in cerium oxide, which was measured as 0.020±0.002 μg/ml. GCCNP had no cytotoxic effect and showed improvements on dry eye disease models by stabilizing the tear film, scavenging ROS, up-regulating SOD, promoting and maintaining corneal and conjunctival cell growth and integrity. We provided convincing evidence that GCCNP is an effective treatment for DE and may represent a potential new class of drug for DE disease.

Graphical abstract

*Correspondence: Zongchao Han, MD, PhD, Department of Ophthalmology, the University of North Carolina at Chapel Hill, Chapel Hill, NC, USA. zongchao@med.unc.edu.

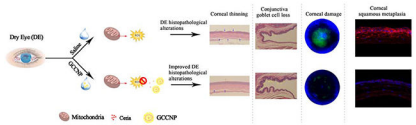

Keywords

Antioxidant nanoparticles; reactive oxygen species (ROS); dry eye disease

1. Introduction

Dry eye syndrome (DE) can result in reduced vision function which can severely impact an individual's quality of life. Currently, about one third of the world's population suffers from this disease, making DE globally recognized as a public health issue [1–5]. DE is a multifactorial disease of the instable and hypertonic tear film caused by reduced tear production, poor tear quality or excessive tear evaporation [6]. Although the pathogenesis of DE remains not well understood, the exposure of oxidative stress to the ocular surface results in associated overproduction of reactive oxygen species (ROS), which have been generally believed to be a main contributor to the development of DE [6–10]. Especially, with the advancement and usage of electronic mobile devices, the increase to light exposure and atmospheric oxidative damage has been investigated as possible contributors to the addition of oxidative stress on the ocular surface, and recognized as the main reasons involved in the pathophysiology of DE [9, 11] [12, 13]. The relationship among ROS production, lipid peroxidation-related membrane damage, protein oxidation, and inflammation has been demonstrated in animal models and in clinical studies. [14, 15]. Under normal biological circumstances, ROS have played an important role in redox regulation of mitochondrial oxidative phosphorylation and have been balanced by biological antioxidant systems. However, long-term exposure to oxidant stress will result in over produced ROS, which cannot be eliminated by antioxidant defense systems. As a result, ROS can be accumulated in the conjunctiva and tear film of DE patients, causing lacrimal gland functional damage. The loss of lacrimal gland function associated with oxidative stress and aging is accelerated by increased mitochondrial superoxide production, which further increase the damage to proteins, lipids, and even DNA on the ocular surface of the dry eye [16].

Continuous deleterious oxidative processes result in ocular surface inflammation and tear film hyperosmolarity, this phenotypic combination may eventually cause DE. There is a suspected cause-and-effect relationship between the increase in ROS production and DE onset/progression. Therefore, scavenging overproduction of pathological ROS becomes a novel strategy that may improve the treatment DE. Antioxidants adopted in the treatment of DE have shown benefit in alleviating DE symptoms in animal models and patients [17–19], indicating that scavenging overproduced ROS holds the promise of developing a solution for the treatment of DE.

Currently, therapeutic approaches for DE have been focused on alleviating symptoms, reducing ocular surface inflammation, and improving the stability of the tear film. Tear

replacement (e.g., artificial tears and lubricants) is currently one of the most commonly used method of treatment for DE. However, these medicines can only temporarily relieve the symptoms by wetting and lubricating the ocular surface in a very short amount of time and cannot treat DE fundamentally [20, 21]. Cerium oxide nanoparticles (CNP) is a unique redox-active system because of possessing +3 (electron donor) and +4 (electron acceptor) valence at same time. CNP have the power to oxidize Ce3+ to Ce4+ acting as a ROS scavenger and resulting in reducing cell injury when exposed to ultraviolet light or H_2O_2, increasing lifespan, and protecting normal cells from radiation-induced apoptosis[22]. Moreover, different from other rare earth elements, CNP possess a high hydrogen-absorbing capacity as a regenerative catalyst, allowing it to react with H_2 or H_2O more easily [22]. Due to this distinctive and inherent redox-active behavior, CNP can eliminate oxidative stress, imitate superoxide dismutase and catalase [23–26] to scavenge ROS, and restore the balance between ROS production and antioxidative enzymes. In preclinical studies, CNP have shown useful ability in the treatment of neurodegenerative disorders and other diseases in which oxidative stress acts as a free radical scavenger [27–30], illustrating prospective scavenging capacity of intracellular ROS and good biocompatibility. Moreover, CNP can promote cell growth, restore tissue damage, which aids in the protection against dysfunction by attenuation of oxidative stress [31, 32]. These inherent properties of CNP are particularly relevant in the context of ROS-induced ocular damage, which may potentiate CNP as an ideal therapeutic drug for DE.

Glycol chitosan (GC) is a water-soluble chitosan derivative. GC has attracted a great deal of attention in the fields of biomedicine due to its non-toxic, biocompatible, and water-soluble characteristics. Our group has previously developed a water-soluble GCCNP [26]. In the present study, we aimed to use this redox-active system to treat DE. We focused on investigating the effects of GCCNP to treat DE both *in vitro* and *in vivo*, using mice primary corneal and conjunctiva cells associated with DE and DE murine models to evaluate the treatment effect. Moreover, Lifitegrast (Xiidra), a U.S. Food and Drug Administration (FDA) approved commercially available DE drug, was adopt as control [33].

2. Materials and methods

2.1. Materials and animals

Glycol chitosan (GC, degree of polymerization ≥400, #G7753), cerium (III) chloride, RPMI medium 1640 (1×), DMEM/F12+GlutaMAX™-I (1×) medium, Improved MEM (Richter's modified) medium, antibiotic-antimycotic solution (100×), and 0.5% Trypsin-EDTA (1×) were purchased from Gibco Life Technologies (Grand Island, NY, USA). Fetal bovine serum (FBS) was purchased from Invitrogen (Carlsbad, CA, USA). All experiments were carried out and animals were maintained in accordance with the Association for Research in Vision and Ophthalmology (ARVO) statement for the use of animals in ophthalmic and vision research and the guidelines of the University of North Carolina at Chapel Hill Animal Care and Use Committee.

2.2 Preparation of GCCNP nanosystem

The CNPs and GCCNPs were prepared according to previous article [25] with slight modifications. Briefly, 0.2 mL of 0.67 M $CeCl_3 \cdot 7H_2O$ (Sigma) solution was added into a 5 mL of 1% (w/v) GC (Sigma) solution with continuous stirring for 15 min to obtain a transparent mixture. 0.3 mL ammonium hydroxide (Sigma, 28–30%) was added into the mixture drop wise. The mixture was reacted at room temperature for 12 h under stirring. Then centrifuged at 4000 rpm for 10 min, the clear supernatant was dialyzed (Thermo Fisher Scientific, 20 kDa MWCO cutoff) for 2 days against distilled water and lyophilized. CNP and blank glycol chitosan nanoparticle were prepared parallel to GCCNP following the same methodology, respectively.

2.3 Characterization

After preparation, the GCCNP were characterized by several analytical techniques. The morphology was observed by transmission electron microscopy on a JEOL 2010F-Fas TEM (TEM, JEOL, Japan) and Asylum Research (ARC2) AFM (AFM, Asylum Research, Abingdon, UK) at UNC Chapel Hill. The hydrodynamic diameter and zeta potential of the GCCNP were determined by dynamic light scattering (Nano-ZS Zeta Sizer, Malvern, USA). A XD-3A powder diffraction meter was adopted to obtain physicochemical properties. IR spectra (Nicolet 2000 , Thermo Electron Corp., Madison, WI) were also used to identify the structure of the formulations mentioned above.

2.4 ICP-MS

Cerium determination was performed by using PerkinElmer NexION 300D coupled plasma mass spectrometers (ICP-MS) (NexION 300D, Perkin Elmer, Waltham, MA). Decomposition of the samples matrix was performed by heating it at 70 °C for 20 h after the addition of HNO_3. After digestion, the sample was adjusted to a proper concentration with deionized (DI) water and analyzed by ICP-MS. Five replicates were analyzed per sample. Quantification was performed by Tb as internal standard.

2.5 Determination of entrapment efficiency and drug-loading

The entrapment efficiency (EE) and drug-loading (DL) of the cerium in GCCNP were analyzed using ICP-MS. The results were calculated according to the following equations:

$$EE(\%) = \frac{\text{Weight of cerium oxide in GCCNP}}{\text{Weight of cerium oxide fed initially}} \times 100\%$$

$$DL(\%) = \frac{\text{Weight of cerium oxide in GCCNP}}{\text{Weight of GCCNP}} \times 100\%$$

2.6 Solubility study

The solubility of CNP or GCCNP in water was analyzed by adding excess amount of CNP or GCCNP into water, then the suspension was placed on a shaking incubator (100 rpm/min) (Fuma; Shanghai, China) at 25 °C for 48h. The solution was centrifuged at 4000 rpm for 10

min, the concentration of cerium oxide in the supernatant was analyzed by ICP-MS after digestion and appropriate dilution according to the method above mentioned.

2.7 Primary corneal cell and conjunctival cell culture

C57BL/6 mice (Jackson Laboratory, ME, USA), aged 8 to 10 weeks, were used to obtain primary corneal cells and conjunctival cells. Primary corneal cell culture was performed according to Hazlett and Ma's reports with modification [34, 35]. After mice are euthanized, via cervical dislocation, eye globes were enucleated then washed in phosphate-buffered saline (PBS). The cornea was cut from the eye and uniformly plated on a tissue culture plate with the epithelium side up. After attachment of the explant, improved MEM (Richter's modified) medium (Gibco, Life Technologies) supplemented with 10% fetal bovine serum (FBS, Gibco, Life Technologies) and 1% Antibiotic-Antimycotic (Gibco, Life Technologies) was added to the plate. Then incubated at 37 °C, under 95% humidity and 5% CO_2, medium was changed every 3 to 4 days. After cells attached to the plate, the explant was gently removed from the plate surface. Cells derived from tissue were also used for subcultures. Corneal cells were subcultured at 1:2 splits after reaching a subconfluence, and the medium was changed every 3 to 4 days. The procedure was repeated until passage (P) 5 cultures. Conjunctiva was cultured using the same method; however, the improved MEM medium was changed to a DMEM medium which was supplemented with 10% FBS and 1% Antibiotic-Antimycotic.

2.8 Cell viability assay

Cell viability was determined using MTT method [36, 37]. Primary corneal cells (5×10^3)/well and conjunctiva cells (8×10^3)/well were seeded plates (Corning, USA) and incubated overnight in a cell culture incubator (Thermo Fisher Scientific, USA) at 37°C. Subsequently, the cells were treated with either different concentrations of GCCNP (0.1, 1 and 10 μM) dissolved in the corneal or conjunctival medium respectively for another 24 or 48 hours. Subsequently, the medium was changed to fresh medium and 10 μL of MTT (5 mg/mL).The plate was incubated for another 4 hours in a CO_2 incubator. After that, purple formazan dye was extracted with 150 μL of DMSO (Sigma, Cat. No. D2650). The optical density (OD) was determined at 570 nm using a microplate reader (FLUOstar Omega, BMG labtech). The cell viability was calculated according to the following equation.

$$\text{cell viability}(\%) = \left(\frac{OD_{\text{treated cells}} - OD_{\text{background}}}{OD_{\text{untreated cells}} - OD_{\text{background}}}\right) \times 100\%$$

2.9 Determination of intracellular ROS

The intracellular ROS was determined using oxidation of 2,7-dichlorodihydrofluorescein diacetate (DCF-DA) (Sigma) to fluorescent 2',7'-dichlorofluorescein (DCF) intracellularly. Briefly, primary corneal cells or primary conjunctival cells were cultured in fresh media containing different concentrations of GCCNP (0.1, 1 and 10 μM) for 24 hour. The next day, the cells were washed twice with 1×DPBS. The fresh culture medium containing 50 μM DCF-DA was added and incubated for 60 min at 37 °C. The solutions were then removed,

fresh medium containing 400 μM H_2O_2 was added and incubated for another 2 h at 37 °C. The cells were washed with 1×DPBS and digested with 0.5% Trypsin-EDTA (Grand Island, NY, USA). The suspended cells were then washed and suspended. GCCNP-untreated cells and H_2O_2-untreated cells remained as a negative control. Cells treated with H_2O_2 and left untreated by GCCNP were taken as positive controls. The DCF fluorescence was measured on flow cytometry (Attune NxT, Thermo Fisher Scientific, US) with excitation and emission wavelength at 485 and 530 nm.

The cells were pretreated with GCCNP (0.1, 1 or 10μM) for 24 hour before exposure to H_2O_2 (400 μM in medium) for 2h. GCCNP-untreated and H_2O_2 –untreated cells remaining as negative control, while GCCNP-untreated and H_2O_2 –treated cells were taken as positive controls. All the GCCNP-pretreated and H_2O_2-treated cells were taken as test group. All these groups were used in other *in vitro* analyses, and each assay was performed in triplicate.

2.10 Measurement of mitochondrial membrane potential

Mitochondria are among the most essential cellular organelles, supplying the indispensable energy for maintaining cellular physiological activities and functions. Mitochondrial membrane potential is a key characteristic about mitochondria and their function. The JC-1 is a well-known fluorescent dye that can change the emission wavelength depending on the mitochondrial membrane potential. JC-1 was adopted to evaluate whether GCCNP altered mitochondrial function in primary corneal and conjunctival cells subjected to H_2O_2-induced oxidative stress [38]. GCCNP pretreated and H_2O_2-treated corneal or conjunctival cells were incubated with 2 μM JC-1 (Thermo Fisher) for 30 minutes. Then the cells were washed with 1×DPBS and digested with 0.5% Trypsin-EDTA (Grand Island, NY, USA). The suspended cells were washed and suspended. Flow cytometry was adopted to quantify JC-1 fluorescence. JC-1 dynamically exist in two different states, aggregates or monomers, which depend on the mitochondrial membrane potential. When the mitochondrial membrane potential is low, JC-1 exists as a monomer and yields green fluorescence (FL-1, Ex510), whereas when the mitochondrial membrane is high, JC-1 monomers aggregate to form the aggregates - these can be observed as red fluorescence (FL-2, Ex585). The relative percentage of red fluorescence to the red and green fluorescence was calculated. Each assay was performed in triplicate.

2.11 *In vitro* cellular uptake

Primary corneal and conjunctival cells were evaluated for the uptake of GCCNP. For visualizing the uptake process of GCCNP by the cells, GCCNP was labeled with Alexa Fluor™ 488 NHS Ester (Life Technologies) according to the protocol. Briefly, 2 mg GCCNP (1mg/ml) were reacted with 5μl AF488 TFP ester (1mg/ml) overnight at room temperature. Then unreacted AF488 molecules were removed by dialysis (MWCO= 14, 000) against distilled water. The solutions were lyophilized. Corneal or conjunctival cells were treated by AF 488 labeled GCCNP solutions for 1,3,5,7 days, then fixed with 4% paraformaldehyde in 1X PBS for 15 min at RT. After washing with 1X HBSS, 2 ml 5μg/ml wheat germ agglutinin AF 647 Conjugate (WGA, W32466, Life Technologies) was applied to cover the cells, then incubated for 10 minutes at RT. Cells were washed twice in HBSS, then mounted with Prolong Gold mounting media with DAPI (Life Technologies). The cells

were observed by using a Zeiss LSM 710 spectral confocal laser scanning microscope (Zeiss, Germany). For flow cytometry, the cells were washed with 1×DPBS and digested with 0.5% Trypsin-EDTA (Grand Island, NY, USA) at the indicated time point. The suspended cells were then washed and suspended for quantitative analysis. The experiment was carried out in triplicate.

2.12 Protein extraction and western blotting

Cells were lysed in extraction buffer (PBS pH 7.0 containing 1% triton-X 100, 5 mM EDTA, 5 mg/ml n-ethylmaleimide, and a standard protease inhibitor cocktail). Lysate was centrifuged at 4°C and supernatants were collected on ice. Protein levels were measured by using Bio-Rad protein assay kit (colorimetric protein assay, Bradford assay, Bio-Rad, Hercules, CA) [39]. The anti-dependent superoxide dismutase (SOD2) (66474-1-Ig) antibodies were purchased from Proteintech (66474-1-Ig, SOD2 Mouse McAb, Proteintech Group, Inc., Rosemont, USA). Whole cell proteins (30 μg each) were separated by SDS-PAGE and transferred to PVDF membrane according to the protocol. The SOD2 protein expression was detected using primary antibody SOD2 (1:20, 000) and HRP conjugated goat anti-mouse IgG antibody (sc-2030, Santa Cruz) at 1:1, 000. Beta-actin (A3854, Sigma-Aldrich) was used as loading control. The experiment was carried out in triplicate.

2.13 Would healing

In vitro primary corneal and conjunctival migration assay were performed in this study [40, 41]. Briefly, primary corneal cells or primary conjunctival cells were seeded and incubated overnight. The next day, three separate straight line scratches (per well) were prepared on the monolayer of primary corneal or conjunctival cells with a sterile pipet tip, cells then washed with 1×DPBS three times. GCCNP (0.1, 1 and 10μM) were added to the different wells. The plate was then incubated in a culture incubator at 37 °C for a period of time. Images of the scratches were taken before and after incubation. Each experiment was done in triplicate.

2.14 Creation of mouse model

All experimental animals were housed in AAALAC-accredited Center for Experimental Animal under sterile environments at the University of North Carolina at Chapel Hill (UNC-CH), and experiments were carried out according to the principles approved by UNC-CH Institutional Animal Care and Use Committee. Briefly, female C57BL/6J mice aged 6 - 8 weeks were housed on an air draft and 30% ambient humidity one week before the experiment start date. Mice were also housed and maintained on an air draft at 30% ambient humidity during the entire duration of the experiment. 0.5 mg/0.2 mL scopolamine hydrobromide (Sigma-Aldrich Corp.) was subcutaneously injected four times a day (8 AM, 11 AM, 2 PM, and 5 PM) to create a DE murine model [42]. The mice were separated at random into six groups (n=6 per group) as follows: (1) DE group, DE mice without treatment; (2) Saline group, DE mice treated with saline; (3) 0.1 μM GCCNP group; (4) 1 μM GCCNP group; (5) 10 μM GCCNP group, and (6) DE mice treated with Xiidra (5% lifitegrast ophthalmic solution, Shire US Inc.). Two μL eye drops were superficially administered to the ocular surface twice a day (9 AM and 5 PM) (Table S1) for 7 days. Clinical gold standard for diagnosis of DE, such as tear volume, tear film break-up time

(TBUT), and corneal fluorescein staining scores were evaluated at different times. The measurements were made 3 hours after the last scopolamine injection and eye drop application. All experiments were repeated three times and performed in triplicate.

2.15 Tear volume

Tear volume were adopted using cotton threads (Zone-Quick, Oasis, Glendora, CA, USA) according to the instruction [43]. The threads were placed on the peripheral conjunctiva at the lateral canthus for 20 seconds after the lower eyelid was pulled down slightly. The thread got red when it was wet by tears, the length of red thread indicated the tear volume, and length of red thread was measured using a microscope (Carl Zeiss, Norway). Each eye was measured three times.

2.16 Evaluation of TBUT and corneal fluorescein staining

The TBUT and staining scores were evaluated according to [42]. For TBUT, 1 μL of 1% sodium fluorescein was instilled into the inferior conjunctiva. TBUT was evaluated under a slit-lamp biomicroscopy (Phoenix Research Laboratories, Pleasanton, CA) equipped with a cobalt blue light. The time of appearance of the first dry spot after the last blink recorded as TBUT. For fluorescein staining, corneal epithelial damage was evaluated by the staining on the corneal surface after instillation 90 seconds. Cornea was divided into four quadrants. The level of corneal fluorescein staining was determined as follows: 0, no staining; 1, slight, micropunctate staining, <30 spots; 2, >30 punctate staining spots without diffuse staining; 3, severe diffuse staining without positive plaque; and 4, severe plaque/patch staining. The total scores of the four quadrants were summed as a final corneal fluorescein staining score. Each eye was measured three times.

2.17 Histological evaluation

On the 7^{th} day, the eyes from different group were collected and fixed in 10% formalin. The specimens were embedded in paraffin after dehydration, cross-sectioned and stained with hematoxylin eosin according to the standard protocol. The morphologies of the corneal, conjunctiva epithelium and goblet cells were observed using a microscope (IX71, Olympus Corp., Tokyo, Japan). Each eye was measured three times.

2.18 Immunofluorescent staining

Cryosections stained for cytokeratin 10 (K10) was developed using donkey anti-mouse Alexa-Fluor 488 conjugated IgG antibody [44]. Eyes were collected on day 7 [44, 45]. Immunofluorescent staining was performed on cryosections. Sections were fixed in acetone at −20 °C. After washing with 1X PBS, blocked with blocking buffer (5% BSA/PBS, 1.0% Triton X-100, 2% donkey serum) for 1 hour, then incubated overnight at 4°C with mouse-anti cytokeratin 10 (1:400, PA5-97907, Millipore) or SOD-2 monoclonal antibody (1:400, 66474-1-Ig, proteintech). Slides were washed with 1X PBS (3x, 10 minutes), incubated with a secondary antibody (1:1000 donkey-anti-mouse Alexa-Fluor 555 for cytokeratin 10, 1:1000 donkey-anti-mouse Alexa-Fluor 555 for SOD-2, Life Technologies), sections were washed again before counterstained with DAPI (Prolong® Gold mounting media, Life

Technologies, USA), and photographed using a confocal laser scanning microscope (Zeiss LSM 710, Germany).

2.19 Statistical analysis

The data were presented as the means ± SEM (n=3). The data were carried out with GraphPad Prism 5.0 software (La Jolla, CA, USA) using Student's t-test or ANOVA with Bonferroni's post-hoc test. A P value of < 0.05 was considered statistically significant.

3. Results

3.1 Characterization of GCCNP

TEM is an electron microscopy in which a beam of electrons is transmitted through a specimen to form a photo. Different components possess different electron transmission capacities. Hence TEM can directly show the different components of the specimen(s) being observed. The representative TEM imaging of GCCNP (Figure 1A) showed that GCCNP are smooth spherical particles with a diameter of around 100 nm. Moreover, the black dots (red arrow) in the figure represent the nano cerium oxide, which were encapsulated by GC. Because cerium oxide has a higher density than GC, the ability of electrons to transmit through nano cerium oxide is more restricted. This is why in TEM imaging, the cerium oxide appears darker than GC. In order to gain better understanding of GCCNP, AFM was adopted to characterize GCCNP. AFM (Figure 1B) revealed that GCCNPs are smooth spherical nanoparticles. The data of dynamic light scattering (DLS) showed that the size of GCCNP was 184.9±8.7 nm (Figure 1C), DLS result are much bigger than TEM's and AFM's. The deviation between the results could be due to the fact that TEM and AFM required the specimen to be dehydrated prior to imaging. GCCNP shrink upon dehydration, resulting in a smaller molecule diameter. Zeta potential of GCCNP was +40.9±3.6 mv (Figure 1C), which indicated that the positively charged GC could be situated on the outer layer of the GCCNP, the result was consistent with TEM's. Moreover, the positive charged surface of GCCNP can not only provide an effective repelling force between the particles to increase the stability, but can also be absorbed by the negative force of the eye globe after its application into eye. This attraction of charge aids in the facilitation of the cellular uptake of GCCNP.

The EE and DL of GCCNP were also investigated. The high EE (80.24±3.9%) and DL (23.18±1.4%) confirm that GC is very suitable as a nano-carrier for cerium oxide.

IR results showed that some characteristic peaks of cerium oxide were weakened or even vanished in the GCCNP, such as 1508.14 and 1338.42 cm^{-1} (Figure 1D). The spectrogram of GCCNP was different from that of cerium oxide in the physical mixture, it was more similar to the spectrogram to GC, which indicated that cerium oxide was encapsulated by GC. The XRD spectrum of GCCNP was similar to that of the blank GC. As shown in Figure 1E, there were several peaks of nano cerium oxide at 28.29°, 33.17°, 47.28° and 56.32° while the characteristic peak of GC was a wide and obtuse peak around 20°. Characteristic peaks of nano cerium oxide were found in the pattern of the physical mixture, while they were vanished in the pattern of GCCNP. A new wide and obtuse peak disappeared at

20.40°in the pattern of GCCNP, which suggested that nano cerium oxide was enclosed by the aggregated structure of GC in the nanoparticle in molecular or amorphous states. This further supports the absence of free cerium oxide in the GCCNP (Figure 1F–I).

3.2 Solubility study

The solubility of CNP and GCCNP were compared. The solubility of cerium in GCCNP increased from 0.020±0.002 μg/ml to 709.854±24.3 μg/ml compared with that of CNP. The solubility of cerium in GCCNP is 35,493 times more soluble than that of the cerium in water. Nano CNP is hydrophobic, while GC is hydrophilic. The hydrophobic nano CNP is surrounded by a hydrophilic GC, which not only increase the hydrophilic effect, but also forms a protective interface to inhibit cerium oxide from precipitating. Therefore, GCCNP can increase the solubility of cerium oxide greatly.

3.3 Tissue preparation and cell culture

In order to achieve results resembling those in the *in vivo* experiment, mouse corneal and conjunctival cells were adopted to do the following tests (Figure 2A and 2B). Cultivation and serial transfer of primary corneal epithelial cells and primary conjunctival cells were adopted under the following conditions. Corneal or conjunctival cells were cultured on type-I collagen (Sigma-Aldrich, USA) coated dishes in IMEM or DMEM with 10% FBS, continued to proliferate until at least P10. The corneal and conjunctival cells appearances did not change throughout the 10 passages.

3.4 Cell viability assay

As illustrated in Figure 2C and 2D, treatment with GCCNP at the indicated concentrations (0.1, 1 and 10 μM) had no significant influence in the primary corneal and conjunctival cells viability, which indicated that GCCNP were noncytotoxic to mouse primary corneal and conjunctival cells.

3.5 Determination of intracellular ROS

Intracellular ROS was quantified by using a sensitive marker, DCF-DA, which can response to the cellular oxidation processes rapidly and determines the ROS in cells by oxidation of non-fluorescent DCF-DA to highly fluorescent DCF intracellularly. The fluorescence intensity of DCF was an indication of the intracellular ROS. Under long term exposure to high levels of ROS, the body's natural defense systems against harmful oxidative species are easily offset, which can lead to a variation of diseases [46, 47]. To determine the ROS scavenging effect of GCCNP on DE *in vitro* models, we evaluated the generation of ROS in corneal and conjunctival cells by flow cytometry. The gating strategy is based is based on the principles of removal of noise signals from air bubbles and disturbing debris to identify single cells. These two cells groups are substantially effected by DE factors. There is a significant decrease in the DCF fluorescence at 1.0 μM and 10 μM GCCNP groups compared to the H_2O_2-positive control, which demonstrated an obvious inhibition effect of 1.0 μM and 10 μM GCCNP (***$P < 0.0001$) on ROS compared to the untreated positive control in Figure 3. The results clearly show that 1.0 and 10 μM GCCNP can drastically scavenge intracellular ROS in corneal and conjunctival cells.

3.6 Measurement mitochondrial membrane potential

Mitochondria are best known as the cellular “power house”, creating and supplying the majority of the cells energy. Mitochondrial membrane potential is a very important index during ROS production. Oxidative stress is always accompanied with the change in mitochondrial membrane potential, which is associated with ROS production and apoptosis (Figure S1). For further exploration of the antioxidant capacity of GCCNP, the mitochondrial membrane potential of the primary corneal and conjunctival cells were measured using JC-1 staining to judge the intracellular oxidative stress. A reduction in the red fluorescence percentage means a decrease of mitochondrial membrane potential. The red fluorescence signal markedly reduced (both in corneal and conjunctival: $p < 0.001$ versus H_2O_2 control), whereas GCCNP-pretreatment significantly increased the red fluorescence percentage compared to the result of the H_2O_2 positive control (corneal: 10 μM GCCNP vs. H_2O_2 positive control, $p < 0.01$; conjunctival: 10 μM GCCNP vs. H_2O_2 positive control, $p < 0.016$). The 10 μM GCCNP and negative control groups did not show a significant difference in the percentage of red fluorescence (cornea: 10 μM GCCNP vs. negative control, $P > 0.05$; conjunctiva: 10 μM GCCNP vs. negative control, $p > 0.05$) Figure 4.

3.7 *In vitro* cellular uptake

After confirming the physicochemical properties of GCCNP, we sought to determine the capability of corneal and conjunctival cells to uptake GCCNP. Uptake behavior was conducted by using a AF488 fluorescent marker. The results are shown in Figure 5 AB. Both primary corneal and conjunctival cells incubated with the GCCNP-AF488 exhibited fluorescence after 1,3,5,7 day’s incubation. Quantitative flow cytometry analysis was performed on the same setting. The results were consistent with those obtained from the microscopy results (Figure 5 CD). In our experiment, the cells were incubated and the fluorescence intensity of those cells were directly related. This direct relationship indicates that the amount of GCCNP entering into cells is indicative to time. The fluorescence intensity on the 5^{th} day was approximately equal to that of the 7^{th} day. Moreover, the intracellular fluorescence of GCCNP-AF488 was mainly distributed in the cytoplasm, which indicated the localization of GCCNP in cytoplasm. As we know, mitochondria are major producers of ROS and are distributed throughout the cytoplasm. Therefore, GCCNP can deliver ceria to the optimal location, clearing excess ROS produced by mitochondria. All the results manifest the ability of primary corneal and conjunctival cells to uptake GCCNP, where our nanoparticles will reside in the preferred intracellular location for the clearing of ROS.

3.8 Protein extraction and western blotting

SOD2 is a well-known protector from ROS in the oxidative stress-related disease. The overexpression of SOD2 attenuates oxidative stress and further reduces apoptosis and mitochondrial dysfunction[48]. CNP have demonstrated the ability to induce the overexpression of SOD2 in colonic crypt cells[32]. However, there was no report about that CNP changes the expression of SOD2 in corneal and conjunctival cells. We explored the effects of GCCNP on the SOD2 in primary corneal and conjunctival cells, in order to investigate the relationship between GCCNP and SOD2. We were eager to study the ability

of GCCNP formulation in the up-regulation of the SOD2 expression in the primary corneal and conjunctiva cells treated with H_2O_2. The corneal cells and conjunctival cells were treated with different concentrations of GCCNP (0.1, 1.0, and 10 μM) for 48 h. After treatments, the cells were further exposed to H_2O_2 (400 μM) for 2 h at 37 °C and 5% CO_2. The protein analysis shows that H_2O_2 down-regulated intracellular SOD2 expression, while different concentrations of GCCNP working against H_2O_2, induced intracellular SOD2 expression. (Figure 6). The results of the quantitative analyses showed that GCCNPs (0.1, 1, 10 μM) significantly increases the intracellular SOD2 expression in primary corneal cell compared with the positive control (without GCCNP-treated but with H_2O_2 treated). This result indicated that even a small amount of GCCNP can upregulate the expression of SOD2 in corneal cells. Meanwhile, in primary conjunctival cells, GCCNP at 10 μM also significantly increases ($*p < 0.05$) the SOD2 expression compared with positive control, showing a comparable expression with the negative control (without GCCNP and H_2O_2 treatment). This evidence shows the ability of GCCNP to act as both a major antioxidant in the treatment of DE and as a transcriptional regulator for the up-regulation of SOD2 expression, proving its extraordinary dual capability.

3.9 Wound healing

Wound healing is a critical component in the restoration of damaged tissue. Therefore, we explored wound healing response of primary corneal and conjunctival cells to GCCNP (Figure 7). Firstly, a scratch-wound assay on cornea and conjunctiva monolayers were performed. Primary corneal and conjunctival cells have an increased promotion of wound closure rates when treated with GCCNP (10 μM) (corneal: ~85% closure, $*p < 0.05$; conjunctiva: ~64% closure, $***p < 0.001$) compared to the control (Figure 7A and 7B). Due to the difference in growth rate of these two cell lines, (i.e., primary conjunctival cells grow very fast under normal culture conditions; 24 hours is enough. But primary corneal cells grow quite slow, so we extended the time to 48 hour), we have conducted the study at a different timepoint. For further evaluation of the wound healing response of primary corneal and conjunctiva cells under pathological ROS states, the cells were treated with H_2O_2. The treatments with different concentration of GCCNP to corneal and conjunctival cell under an H_2O_2 environment led to different levels of the promotion (Figure 7C and 7D) of wound closures. GCCNP (10 μM)-treated cells greatly promote wound closures in both corneal and conjunctival cells (corneal: ~89% closure, $**p < 0.01$; conjunctiva: ~70% closure, $*p < 0.05$) compared to the control.

3.10 Tear volume measurements

Tear volume is an important index in the evaluation of DE in a clinical setting. Therefore, the effect of GCCNP treatment on the changes of tear volume in DE mice models was investigated. The tear volumes were 0.42±0.054 μL in DE group (Figure 8A). On the contrary, the tear volumes were 0.47±0.066, 0.56±0.14, 0.72±0.15 μL in 0.1, 1, 10 μM GCCNP-treated groups, and the mean tear volume of the Xiidra treated groups were 0.86±0.18 μL. The results indicate that the tear volume increased after 7-day of GCCNP and Xiidra treatment. Compared to the DE group, there was a significant increase in tear volume in the 10 μM GCCNP group, and a very significant increase in Xiidra group. There was no differences in tear volume between 10 μM GCCNP and Xiidra group ($P>0.05$).

3.11 TBUT and corneal fluorescein staining

With exposure to a 30% humidity environment paired with a subcutaneous injection of scopolamine hydrobromide, a successful 'DE' murine model was established. The TBUT and fluorescein staining scores were 6.15±1.26 s and 2.2 ±0.6 before injection of scopolamine, and 1.42±0.31 s and 13.2±1.86 immediately after four rounds of subcutaneous injection with scopolamine hydrobromide in the DE group. Compared to the DE group, TBUT was significantly prolonged in the 10 μM GCCNP and Xiidra groups on the 7^{th} day of treatment. No significant difference between the 10 μM CGC group and Xiidra group was found (Figure 8B).

Fluorescein staining scores were decreased in the DE group on day 7 (Figure 8C), but there was no significant difference compared to day 0 scores ($p > 0.05$). Corneal fluorescein staining scores in the 1 μM GCCNP group were significantly decreased on days 3 and 7, compared to day 0 (* $p < 0.05$). Scores in the 10 μM group were significantly decreased on days 3 and 7, compare to day 0 ($^{\#}$ day 3 vs day 0, $p < 0.05$; $^{\#\#}$day 7 vs day 0, $p < 0.01$). Scores in the Xiidra group were significantly decreased on days 3 and 7, compare to day 0 ($^{\&\&}$ day 3 vs day 0, $p < 0.01$; $^{\&\&\&}$day 7 vs day 0, $p < 0.001$). On day 7, compared with the DE group, there were significant decreases in fluorescein staining scores in the 10 μM group ($p < 0.01$), an significant decreases ($p < 0.001$) in the Xiidra group. However, there was no significant difference between 10 μM GCCNP group and Xiidra group.

Representative fluorescein staining images were shown in Figure 8D, the damage on the corneal surface between the treatment groups is easily evaluated and compared according to the green fluorescence. Positive plaque staining could be clearly observed on the surface of corneal on day 0 in 5 groups, including the DE group, GCCNP (0.1, 1.0, and 10 μM) and Xiidra group, which indicated that a 'DE' murine model was successfully established in every group. On the contrary, only punctate staining was found on 10 μM GCCNP and Xiidra group for 3 days. On the 7 day, plaque staining also observed in the DE group and the 0.1 μM GCCNP group, however, micropunctate staining was hardly found in 10 μM GCCNP and Xiidra groups.

3.12 Histological evaluation

After a one-week exposure to a low humidity environment and four rounds of subcutaneous injection with scopolamine hydrobromide, the 'DE' murine models experienced a change of ocular phenotypes. The thickness of corneal epithelia was distinctly thinner and damaged; the corneal stroma was obviously thinner and looser compared to the normal group, with disorganized layers (Figure 9A). After 7-day of treatment with 10 μM GCCNP and Xiidra, the damaged corneal epithelial layers began to recover, corneal morphology became smooth and returned to a near normal status, with a similar epithelial thickness and stromal morphology.

However, even 10 μM GCCNP did not normalize corneal morphology nearly as well as Xiidra. The corneal epithelial layer treated by 1 and 0.1 μM GCCNP did not recover more than 10 μM GCCNP. However, the morphology of corneal epithelial layer still improved compared with DE group.

The number of goblet cells (as showed by the yellow arrows in Figure 9B) were significantly decreased in the ‘DE’ group compared to that of normal conjunctiva groups. Conjunctiva goblet cells play a very important role in the secretion of tears. The density of goblet cells represents the quantity of tear volume, which is indicative of the degree of development of DE disease. The density of goblet cell were much higher after treatment with 10 μM GCCNP than in the 1, 0.1μM GCCNP and DE groups. In addition, our results also indicated that GCCNP could protect against apoptosis caused by DE as revealed by TUNEL analysis (Figure S1).

3.13 Immunofluorescent Staining and Laser Scanning Confocal Microscopy

Squamous metaplasia is an ocular surface inflammatory disorder, which is an indication of DE [49–52]. The epidermis-specific K10 expression indicates the alteration of squamous metaplasia. To evaluate the expression of K10 on corneal after the treatment of GCCNP, immunohistochemistry with eye globe cryosections were carried out for a duration of 7 days (Figure 10). Normal corneal epithelium was K10 negative, while the epithelia treated with scopolamine hydrobromide were K10 positive. The results showed that the amount of K10 expression in GCCNP-treated groups (0.1, 1 and 10 μM GCCNP) was much weaker than that of the DE group.

4. Discussion

DE is a complex disease, instead of being the result of a direct cause and effect, there are many factors that contribute to the development and progression of the disease. Currently, there are only two drugs (Cyclosporine and Lifitegrast) approved by the FDA in the market, and they are selective in their treatment ability. There is a high-unmet medical need to develop new treatment options for DE. In this study, we developed a new formulation (GCCNP) that has multi-targeted functionalities focusing on oxidative stress factors, which contribute to DE. We have characterized GCCNP formulations and performed comparative toxicity and efficacy evaluations of GCCNP (0.1, 1, 10 μM) to commercially available Xiidra, a drug approved by FDA.

Cerium oxide illustrated prospective scavenging activity of intracellular ROS *in vitro*, however, solubility limited its application *in vivo*. An appropriate material is critical to develop a nanoscale cerium oxide system. We chose GC—a derivation of chitosan as main material, and developed a stable cerium oxide loaded glycol chitosan nanoscale system. Our approach proved that a nanoscale cerium oxide matrix (the dark spots) was successfully embedded in the nanoscale system formed by GC, as illustrated on electron micrographs. The particle size and distribution are very important parameters for a nanoscale system. The smaller the size of the nanoparticles (approximately 100 nm) the better capacity and ability they have to penetrate the cell membrane barriers, thus have a higher uptake compare with larger particles (approximately 800–1000 nm) [53]. This is may also be partially due to the interaction between the positively charged GCCNPs and negatively charged cellular membranes. Studies have also shown that chitosan can transiently open intercellular tight junctions, allowing a chitosan NP-mediated drug delivery system to enter the cell [54, 55]. Moreover, the zeta potential of the GCCNP were around +40 mV, it is more stable because

of the electrostatic repulsion between the particles [56, 57]. The high EE and DL (80.24±3.9% and 23.18±1.4%) approved that GC is suitable for cerium oxide as nano carrier. IR and XRD analysis shown that a series of cerium oxide characteristic peaks weakened in the GCCNP and some peaks even disappeared. The results suggested that cerium oxide was entrapped into the GC. Solubility is a very important aspect in the evaluation of future possible drug use. The solubility of cerium in GCCNP increased from 0.020±0.002 μg/ml to 709.854±24.3 μg/ml. Compared to cerium oxide, GCCNP is therefore more soluble. Toxicity is another aspect to consider when developing a new drug. To better evaluate toxicity and treatment effect of GCCNP, the primary corneal and conjunctival cells that are directly associated with DE were adopted to evaluate in our experiment. As proved by cell viability assay, our results showed that GCCNP have no cytotoxicity to primary corneal and conjunctival cells, even in the highest concentration, thus making it a promising candidate for DE treatment. GCCNP are ROS scavengers, so the effect of GCCNP on ROS scavenging was evaluated. A significant decrease in the DCF fluorescence at 1.0 μM and 10 μM GCCNP compared to the H_2O_2-positive control suggest that 1.0 and 10 μM GCCNP can decrease intracellular ROS greatly in cornea and conjunctiva. The mitochondrial membrane potential is a very important index during ROS production. Any change of the mitochondrial membrane potential indicates that GCCNP could reside in the preferred intracellular location for efficient clearing of ROS. After confirming the uptake of GCCNP in the corneal and conjunctival cells, the effects of GCCNP in up-regulating the SOD2 expression was investigated. Our results showed that GCCNP can up-regulate H_2O_2-induced intracellular SOD expression, indicating that GCCNP not only plays an important role against ROS in corneal and conjunctival cells, but also significantly up-regulates the expression of SOD. Wound healing is a critical step for the recovery of a damaged ocular surface; therefore, we explored the wound healing response of primary corneal cells and conjunctival cells to GCCNP exposure. GCCNP (10 μM)-treated cells promote wound closures in both corneal and conjunctival cells, especially under an H_2O_2 environment, which indicates that GCCNP could help for the recovery of ocular surface damaged in DE disease. Tear volume and TBUT are very important indices to evaluate the development of DE in the clinical setting [58, 59]. The results indicate that the tear volume increased after GCCNP treatment. Compared to the DE group, there was a significant increase in tear volume in the 10 μM GCCNP-treated group. Significantly prolonged TBUT was observed with 10 μM GCCNP compared to the DE group. A longer TBUT commonly means a more stable tear film [60], the results indicate that 10μM GCCNP were helpful in the recovery of the tear film. Fluorescein staining is an effective method to evaluate the damage inflicted by ocular surface associated diseases [61]. The 10μM GCCNP group obtained a significant decrease in corneal fluorescein staining scores compared to 1.0μM CGC group, 0.1μM GCCNP group and DE group. The results of the staining scores were highly consistent with that of the TBUT, both of these results indicated that a higher concentration (10μM) of GCCNP is helpful in restoring the damaged corneal tissue. The function of conjunctival goblet cells is lubrication and protection of the ocular surface by secreting mucoproteins [62]. However, conjunctival goblet cells are very sensitive to ROS. The abnormal increase in intracellular ROS would lead to goblet cells apoptosis. A decrease in conjunctival goblet cells caused by ROS leads to a decrease of mucoproteins, consequently leading to an unstable tear film, and eventually damaging the corneal surface. Therefore, the quantity of goblet cells is very

essential in the treatment of DE. Recovery of corneal epithelial morphology to a normal status is also important during the treatment of DE. In the 'DE' group, the thickness of the corneal epithelia were reduced and the number of conjunctival goblet cells noticeably decreased after creating the model. Nevertheless, after a 7-day treatment period, HE results demonstrated that the corneal was almost completely restored and a normal number of goblet cells, with normal morphology, appeared in the conjunctiva, indicating that GCCNP fundamentally facilitate the creation of a stable tear film. DE is also accompanied by squamous metaplasia, results in an epidermis-specific K10 expression. This K10 expression was indicated by the alteration of squamous metaplasia and the intensity of K10 expression in both GCCNP-treated groups was much weaker than that of the DE groups, suggesting that GCCNP ameliorated corneal epithelium squamous metaplasia is directly caused by DE and can be an effective therapy for the treatment of DE.

5. Conclusions

In summary, GCCNP is a water-soluble cerium oxide formulation which scavenged ROS, up-regulated SOD, promoted mouse corneal and conjunctival cell growth, alleviated ocular surface disease (both *in vitro* and *in vivo*), and showed improvements on DE by stabilizing the tear film, while maintaining the integrity of epithelium. We provided convincing evidence that GCCNP is an effective treatment for DE. Our experiments demonstrate that GCCNP not only ameliorates symptoms but also reverses pathological changes at the cellular and molecular levels in DE. Thus, it represents a potential new class of drug for the treatment of DE.

Supplementary Material

Refer to Web version on PubMed Central for supplementary material.

Acknowledgements

The authors thank Kaitlyn Lee Lester (Department of Ophthalmology, University of North Carolina at Chapel Hill) for her critical reading of the manuscript. We also thank Drs. Rajendra N. Mitra and Kai Wang (Department of Ophthalmology, University of North Carolina at Chapel Hill) for their kind help with the manuscript preparation and analyses. This work was supported by the Natural Science Foundation of Jiangsu Province (Grants No BK20181478, for F.Y.), the Edward N. & Della L. Thome Memorial Foundation (Z.H.), the BrightFocus Foundation (M2019063, Z.H.), the Carolina Center of Cancer Nanotechnology Excellence (Z.H.), and the U.S. National Eye Institute (R01EY026564, Z.H.).

Uncategorized References

[1]. Stern ME, Schaumburg CS, Pflugfelder SC, Dry Eye as a Mucosal Autoimmune Disease, Int Rev Immunol, 32 (2013) 19–41. [PubMed: 23360156]

[2]. Miljanovic B, Dana R, Sullivan DA, Schaumberg DA, Impact of dry eye syndrome on vision-related quality of life, Am J Ophthalmol, 143 (2007) 409–415. [PubMed: 17317388]

[3]. Gayton JL, Etiology, prevalence, and treatment of dry eye disease, Clin Ophthalmol, 3 (2009) 405–412. [PubMed: 19688028]

[4]. Galor A, Feuer W, Lee DJ, Florez H, Carter D, Pouyeh B, Prunty WJ, Perez VL, Prevalence and risk factors of dry eye syndrome in a United States veterans affairs population, Am J Ophthalmol, 152 (2011) 377–384 e372. [PubMed: 21684522]

[5]. Pierce CW, Dry Eye, N Engl J Med, 379 (2018) e19.

[6]. Seen S, Tong L, Dry eye disease and oxidative stress, Acta Ophthalmol, 96 (2018) e412–e420. [PubMed: 28834388]

[7]. Barabino S, Chen YH, Chauhan S, Dana R, Ocular surface immunity: Homeostatic mechanisms and their disruption in dry eye disease, Prog Retin Eye Res, 31 (2012) 271–285. [PubMed: 22426080]

[8]. Zoukhri D, Effect of inflammation on lacrimal gland function, Experimental Eye Research, 82 (2006) 885–898. [PubMed: 16309672]

[9]. Nakamura S, Shibuya M, Nakashima H, Hisamura R, Masuda N, Imagawa T, Uehara M, Tsubota K, Involvement of oxidative stress on corneal epithelial alterations in a blink-suppressed dry eye, Invest Ophthalmol Vis Sci, 48 (2007) 1552–1558. [PubMed: 17389484]

[10]. Zheng Q, Ren Y, Reinach PS, She Y, Xiao B, Hua S, Qu J, Chen W, Reactive oxygen species activated NLRP3 inflammasomes prime environment-induced murine dry eye, Exp Eye Res, 125 (2014) 1–8. [PubMed: 24836981]

[11]. Demir U, Demir T, Ilhan N, The protective effect of alpha-lipoic acid against oxidative damage in rabbit conjunctiva and cornea exposed to ultraviolet radiation, Ophthalmologica, 219 (2005) 49–53. [PubMed: 15627828]

[12]. Hsu SD, Dickinson DP, Qin H, Borke J, Ogbureke KUE, Winger JN, Camba AM, Bollag WB, Stoppler HJ, Sharawy MM, Schuster GS, Green tea polyphenols reduce autoimmune symptoms in a murine model for human Sjogren's syndrome and protect human salivary acinar cells from TNF-alpha-induced cytotoxicity, Autoimmunity, 40 (2007) 138–147. [PubMed: 17364504]

[13]. Higuchi A, Takahashi K, Hirashima M, Kawakita T, Tsubota K, Selenoprotein P controls oxidative stress in cornea, PLoS One, 5 (2010) e9911. [PubMed: 20360971]

[14]. Wakamatsu TH, Dogru M, Tsubota K, Tearful relations: oxidative stress, inflammation and eye diseases, Arq Bras Oftalmol, 71 (2008) 72–79. [PubMed: 19274416]

[15]. Shoham A, Hadziahmetovic M, Dunaief JL, Mydlarski MB, Schipper HM, Oxidative stress in diseases of the human cornea, Free Radic Biol Med, 45 (2008) 1047–1055. [PubMed: 18718524]

[16]. Uchino Y, Kawakita T, Miyazawa M, Ishii T, Onouchi H, Yasuda K, Ogawa Y, Shimmura S, Ishii N, Tsubota K, Oxidative stress induced inflammation initiates functional decline of tear production, PLoS One, 7 (2012) e45805. [PubMed: 23071526]

[17]. Larmo PS, Jarvinen RL, Setala NL, Yang B, Viitanen MH, Engblom JR, Tahvonen RL, Kallio HP, Oral sea buckthorn oil attenuates tear film osmolarity and symptoms in individuals with dry eye, J Nutr, 140 (2010) 1462–1468. [PubMed: 20554904]

[18]. Jarvinen RL, Larmo PS, Setala NL, Yang B, Engblom JR, Viitanen MH, Kallio HP, Effects of oral sea buckthorn oil on tear film Fatty acids in individuals with dry eye, Cornea, 30 (2011) 1013–1019. [PubMed: 21832964]

[19]. Andrade AS, Salomon TB, Behling CS, Mahl CD, Hackenhaar FS, Putti J, Benfato MS, Alpha-lipoic acid restores tear production in an animal model of dry eye, Exp Eye Res, 120 (2014) 1–9. [PubMed: 24394592]

[20]. Lee HS, Choi JH, Cui L, Li Y, Yang JM, Yun JJ, Jung JE, Choi W, Yoon KC, Anti-Inflammatory and Antioxidative Effects of Camellia japonica on Human Corneal Epithelial Cells and Experimental Dry Eye: In Vivo and In Vitro Study, Invest Ophthalmol Vis Sci, 58 (2017) 1196–1207. [PubMed: 28245300]

[21]. Zhang W, Wang Y, Lee BT, Liu C, Wei G, Lu W, A novel nanoscale-dispersed eye ointment for the treatment of dry eye disease, Nanotechnology, 25 (2014) 125101. [PubMed: 24571862]

[22]. Rzigalinski BA, Meehan K, Davis RM, Xu Y, Miles WC, Cohen CA, Radical nanomedicine, Nanomedicine, 1 (2006) 399–412. [PubMed: 17716143]

[23]. Li Y, He X, Yin JJ, Ma Y, Zhang P, Li J, Ding Y, Zhang J, Zhao Y, Chai Z, Zhang Z, Acquired superoxide-scavenging ability of ceria nanoparticles, Angew Chem Int Ed Engl, 54 (2015) 1832–1835. [PubMed: 25515687]

[24]. Heckert EG, Karakoti AS, Seal S, Self WT, The role of cerium redox state in the SOD mimetic activity of nanoceria, Biomaterials, 29 (2008) 2705–2709. [PubMed: 18395249]

[25]. Pirmohamed T, Dowding JM, Singh S, Wasserman B, Heckert E, Karakoti AS, King JE, Seal S, Self WT, Nanoceria exhibit redox state-dependent catalase mimetic activity, Chem Commun (Camb), 46 (2010) 2736–2738. [PubMed: 20369166]

[26]. Mitra RN, Gao RJ, Zheng M, Wu MJ, Voinov MA, Smirnov AI, Smirnova TI, Wang K, Chavala S, Han ZC, Glycol Chitosan Engineered Autoregenerative Antioxidant Significantly Attenuates Pathological Damages in Models of Age-Related Macular Degeneration, Acs Nano, 11 (2017) 4669–4685. [PubMed: 28463509]

[27]. Singh R, Singh S, Role of phosphate on stability and catalase mimetic activity of cerium oxide nanoparticles, Colloids Surf B Biointerfaces, 132 (2015) 78–84. [PubMed: 26011425]

[28]. Heckman KL, DeCoteau W, Estevez A, Reed KJ, Costanzo W, Sanford D, Leiter JC, Clauss J, Knapp K, Gomez C, Mullen P, Rathbun E, Prime K, Marini J, Patchefsky J, Patchefsky AS, Hailstone RK, Erlichman JS, Custom cerium oxide nanoparticles protect against a free radical mediated autoimmune degenerative disease in the brain, ACS Nano, 7 (2013) 10582–10596. [PubMed: 24266731]

[29]. Estevez AY, Erlichman JS, The potential of cerium oxide nanoparticles (nanoceria) for neurodegenerative disease therapy, Nanomedicine (Lond), 9 (2014) 1437–1440. [PubMed: 25253491]

[30]. Ciofani G, Genchi GG, Liakos I, Cappello V, Gemmi M, Athanassiou A, Mazzolai B, Mattoli V, Effects of cerium oxide nanoparticles on PC12 neuronal-like cells: proliferation, differentiation, and dopamine secretion, Pharm Res, 30 (2013) 2133–2145. [PubMed: 23661146]

[31]. Niu J, Azfer A, Rogers LM, Wang X, Kolattukudy PE, Cardioprotective effects of cerium oxide nanoparticles in a transgenic murine model of cardiomyopathy, Cardiovasc Res, 73 (2007) 549–559. [PubMed: 17207782]

[32]. Colon J, Hsieh N, Ferguson A, Kupelian P, Seal S, Jenkins DW, Baker CH, Cerium oxide nanoparticles protect gastrointestinal epithelium from radiation-induced damage by reduction of reactive oxygen species and upregulation of superoxide dismutase 2, Nanomedicine, 6 (2010) 698–705. [PubMed: 20172051]

[33]. Perez VL, Pflugfelder SC, Zhang S, Shojaei A, Haque R, Lifitegrast, a Novel Integrin Antagonist for Treatment of Dry Eye Disease, Ocul Surf, 14 (2016) 207–215. [PubMed: 26807723]

[34]. Ma X, Shimmura S, Miyashita H, Yoshida S, Kubota M, Kawakita T, Tsubota K, Long-term culture and growth kinetics of murine corneal epithelial cells expanded from single corneas, Invest Ophthalmol Vis Sci, 50 (2009) 2716–2721. [PubMed: 19218612]

[35]. Hazlett L, Masinick S, Mezger B, Barrett R, Kurpakus M, Garrett M, Ultrastructural, immunohistological and biochemical characterization of cultured mouse corneal epithelial cells, Ophthalmic Res, 28 (1996) 50–56. [PubMed: 8726677]

[36]. Wang K, Mitra RN, Zheng M, Han Z, Nanoceria-loaded injectable hydrogels for potential age-related macular degeneration treatment, J Biomed Mater Res A, (2018).

[37]. Oliveira CR, Spindola DG, Garcia DM, Erustes A, Bechara A, Palmeira-Dos-Santos C, Smaili SS, Pereira GJS, Hinsberger A, Viriato EP, Cristina Marcucci M, Sawaya A, Tomaz SL, Rodrigues EG, Bincoletto C, Medicinal properties of Angelica archangelica root extract: Cytotoxicity in breast cancer cells and its protective effects against in vivo tumor development, J Integr Med, 17 (2019) 132–140. [PubMed: 30799248]

[38]. Dalal S, Zha Q, Singh M, Singh K, Osteopontin-stimulated apoptosis in cardiac myocytes involves oxidative stress and mitochondrial death pathway: role of a pro-apoptotic protein BIK, Mol Cell Biochem, 418 (2016) 1–11. [PubMed: 27262843]

[39]. Li M, Tang LS, Wu LS, Mo FF, Wang X, Li HX, Qi RR, Zhang HW, Srivastava A, Ling C, The hepatocyte- specific HNF4 alpha/miR-122 pathway contributes to iron overload-mediated hepatic inflammation, Blood, 130 (2017) 1041–1051. [PubMed: 28655781]

[40]. Mitra RN, Nichols CA, Guo J, Makkia R, Cooper MJ, Naash MI, Han Z, Nanoparticle-mediated miR200-b delivery for the treatment of diabetic retinopathy, J Control Release, 236 (2016) 31–37. [PubMed: 27297781]

[41]. Arnaoutova I, Kleinman HK, In vitro angiogenesis: endothelial cell tube formation on gelled basement membrane extract, Nature Protocols, 5 (2010) 628–635. [PubMed: 20224563]

[42]. Sung MS, Li Z, Cui L, Choi JS, Choi W, Park MJ, Park SH, Yoon KC, Effect of Topical 5-Aminoimidazole-4-carboxamide-1-beta-d-Ribofuranoside in a Mouse Model of Experimental Dry Eye, Invest Ophthalmol Vis Sci, 56 (2015) 3149–3158. [PubMed: 26024098]

[43]. Yoon KC, Ahn KY, Choi W, Li Z, Choi JS, Lee SH, Park SH, Tear production and ocular surface changes in experimental dry eye after elimination of desiccating stress, Invest Ophthalmol Vis Sci, 52 (2011) 7267–7273. [PubMed: 21849424]

[44]. Mitra RN, Zheng M, Weiss ER, Han Z, Genomic form of rhodopsin DNA nanoparticles rescued autosomal dominant Retinitis pigmentosa in the P23H knock-in mouse model, Biomaterials, 157 (2018) 26–39. [PubMed: 29232624]

[45]. Zheng M, Mitra RN, Filonov NA, Han ZC, Nanoparticle-mediated rhodopsin cDNA but not intron-containing DNA delivery causes transgene silencing in a rhodopsin knockout model, Faseb Journal, 30 (2016)1076–1086. [PubMed: 26564956]

[46]. Kaczara P, Sarna T, Burke JM, Dynamics of H2O2 availability to ARPE-19 cultures in models of oxidative stress, Free Radic Biol Med, 48 (2010) 1064–1070. [PubMed: 20100568]

[47]. Bailey TA, Kanuga N, Romero IA, Greenwood J, Luthert PJ, Cheetham ME, Oxidative stress affects the junctional integrity of retinal pigment epithelial cells, Invest Ophthalmol Vis Sci, 45 (2004) 675–684. [PubMed: 14744914]

[48]. Keller JN, Kindy MS, Holtsberg FW, Clair DK St, Yen HC, Germeyer A,., Steiner SM, Bruce-Keller AJ, Hutchins JB, Mattson MP, Mitochondrial manganese superoxide dismutase prevents neural apoptosis and reduces ischemic brain injury: suppression of peroxynitrite production, lipid peroxidation, and mitochondrial dysfunction, Journal of Neuroscience, 18 (1998) 687–697. [PubMed: 9425011]

[49]. Murube J, Rivas L, Impression cytology on conjunctiva and cornea in dry eye patients establishes a correlation between squamous metaplasia and dry eye clinical severity, Eur J Ophthalmol, 13 (2003) 115–127. [PubMed: 12696629]

[50]. Xiao XY, Luo PP, Zhao H, Chen JY, He H, Xu YX, Lin ZR, Zhou YP, Xu JJ, Liu ZG, Amniotic membrane extract ameliorates benzalkonium chloride-induced dry eye in a murine model, Experimental Eye Research, 115 (2013) 31–40. [PubMed: 23792171]

[51]. Zgheib C, Hilton SA, Dewberry LC, Hodges MM, Ghatak S, Xu JW, Singh S, Roy S, Sen CK, Seal S, Liechty KW, Use of Cerium Oxide Nanoparticles Conjugated with MicroRNA-146a to Correct the Diabetic Wound Healing Impairment, J Am Coll Surgeons, 228 (2019) 107–115.

[52]. Wu H, Li F, Wang S, Lu J, Li J, Du Y, Sun X, Chen X, Gao J, Ling D, Ceria nanocrystals decorated mesoporous silica nanoparticle based ROS-scavenging tissue adhesive for highly efficient regenerative wound healing, Biomaterials, 151 (2018) 66–77. [PubMed: 29078200]

[53]. Nagarwal RC, Kant S, Singh PN, Maiti P, Pandit JK, Polymeric nanoparticulate system: a potential approach for ocular drug delivery, J Control Release, 136 (2009) 2–13. [PubMed: 19331856]

[54]. Smith J, Wood E, Dornish M, Effect of chitosan on epithelial cell tight junctions, Pharm Res, 21 (2004) 43–49. [PubMed: 14984256]

[55]. Smith JM, Dornish M, Wood EJ, Involvement of protein kinase C in chitosan glutamate-mediated tight junction disruption, Biomaterials, 26 (2005) 3269–3276. [PubMed: 15603822]

[56]. Levy MY, Schutze W, Fuhrer C, Benita S, Characterization of diazepam submicron emulsion interface: role of oleic acid, J Microencapsul, 11 (1994) 79–92. [PubMed: 8138877]

[57]. Yu F, Jiang F, Tang X, Wang B, N-octyl-N-arginine-chitosan micelles for gambogic acid intravenous delivery: characterization, cell uptake, pharmacokinetics, and biodistribution, Drug Dev Ind Pharm, 44 (2018)615–623. [PubMed: 29188736]

[58]. Goto E, Dogru M, Fukagawa K, Uchino M, Matsumoto Y, Saiki M, Tsubota K, Successful tear lipid layer treatment for refractory dry eye in office workers by low-dose lipid application on the full-length eyelid margin, American Journal of Ophthalmology, 142 (2006) 264–270. [PubMed: 16876507]

[59]. Lin Z, Liu X, Zhou T, Wang Y, Bai L, He H, Liu Z, A mouse dry eye model induced by topical administration of benzalkonium chloride, Mol Vis, 17 (2011) 257–264. [PubMed: 21283525]

[60]. O'Brien PD, Collum LM, Dry eye: diagnosis and current treatment strategies, Curr Allergy Asthma Rep, 4 (2004) 314–319. [PubMed: 15175147]

[61]. Bron AJ, Tiffany JM, Gouveia SM, Yokoi N, Voon LW, Functional aspects of the tear film lipid layer, Exp Eye Res, 78 (2004) 347–360. [PubMed: 15106912]

[62]. Watanabe H, Significance of mucin on the ocular surface, Cornea, 21 (2002) S17–22. [PubMed: 11995804]

Highlights:

- The glycol chitosan (GC)-coated cerium oxide (CNP) displayed significantly higher solubility.
- GCCNP can scavenge ROS, up-regulate antioxidant enzyme SOD2, and enhance mitochondrial membrane potential in dry eye (DE) models.
- GCCNP improves tear secretion, tear film stability, and ocular surface integrity.

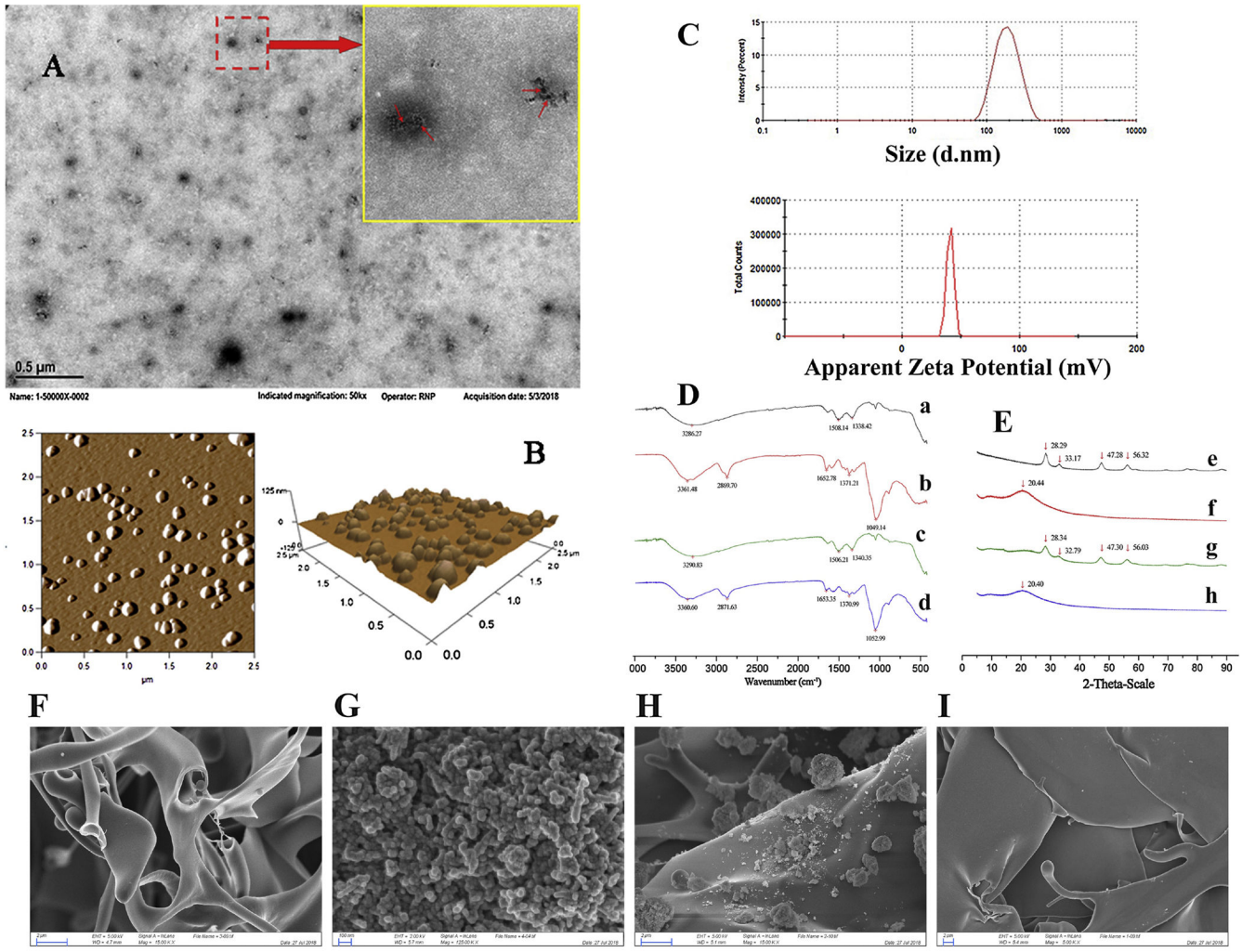

Figure 1.

Characterization of GCCNP eye drop. (**A & B**)TEM and AFM images of GCCNP. (**A**) TEM images. Small red arrow indicates nano ceria. (**B**) AFM images. (**C**) Size and zeta potential of GCCNP. (**D**) IR spectrograms of Cerium oxide (a), GC (b), Mechanical mixture of Cerium oxide nanoparticle (CNP) and GC (c), and GCCNP (d), (**E**) XRD spectrograms of Cerium oxide (e), GC (f), Mechanical mixture of Cerium oxide and GC (g), and GCCNP (h), and (**F-I**) SEM images (**F**: GC, **G:**CNP, **H:** Mechanical mixture of GC and CNP, and **I:** GCCNP).

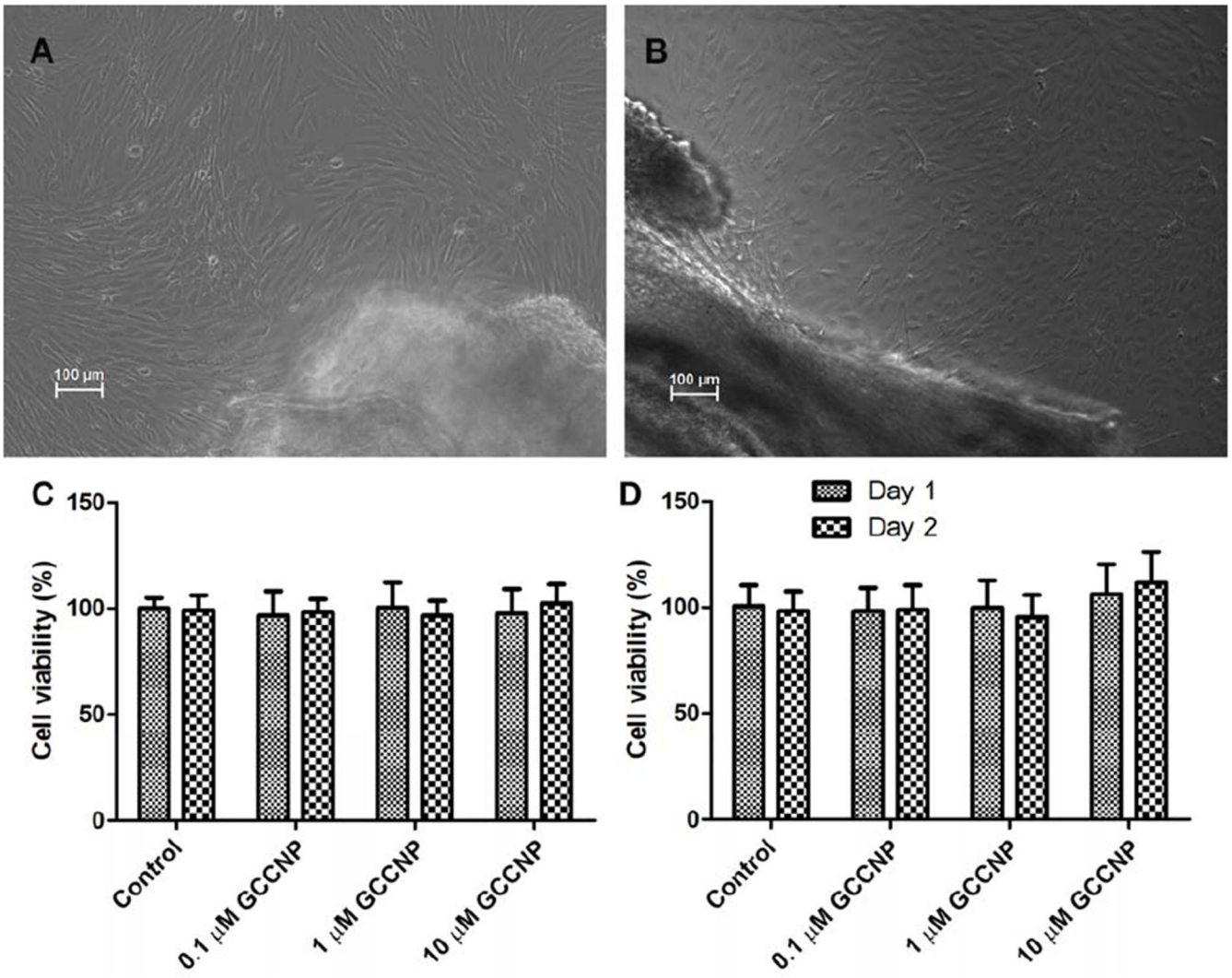

Figure 2.

(**A**) Mouse corneal and (**B**) conjunctival primary cultures. (**C**) Corneal and (**D**) Conjunctival MTT assays. Results are presented as means ± SEM from three parallel samples. There was no significant difference in the viability of cells exposed to the GCCNP compared to the control.

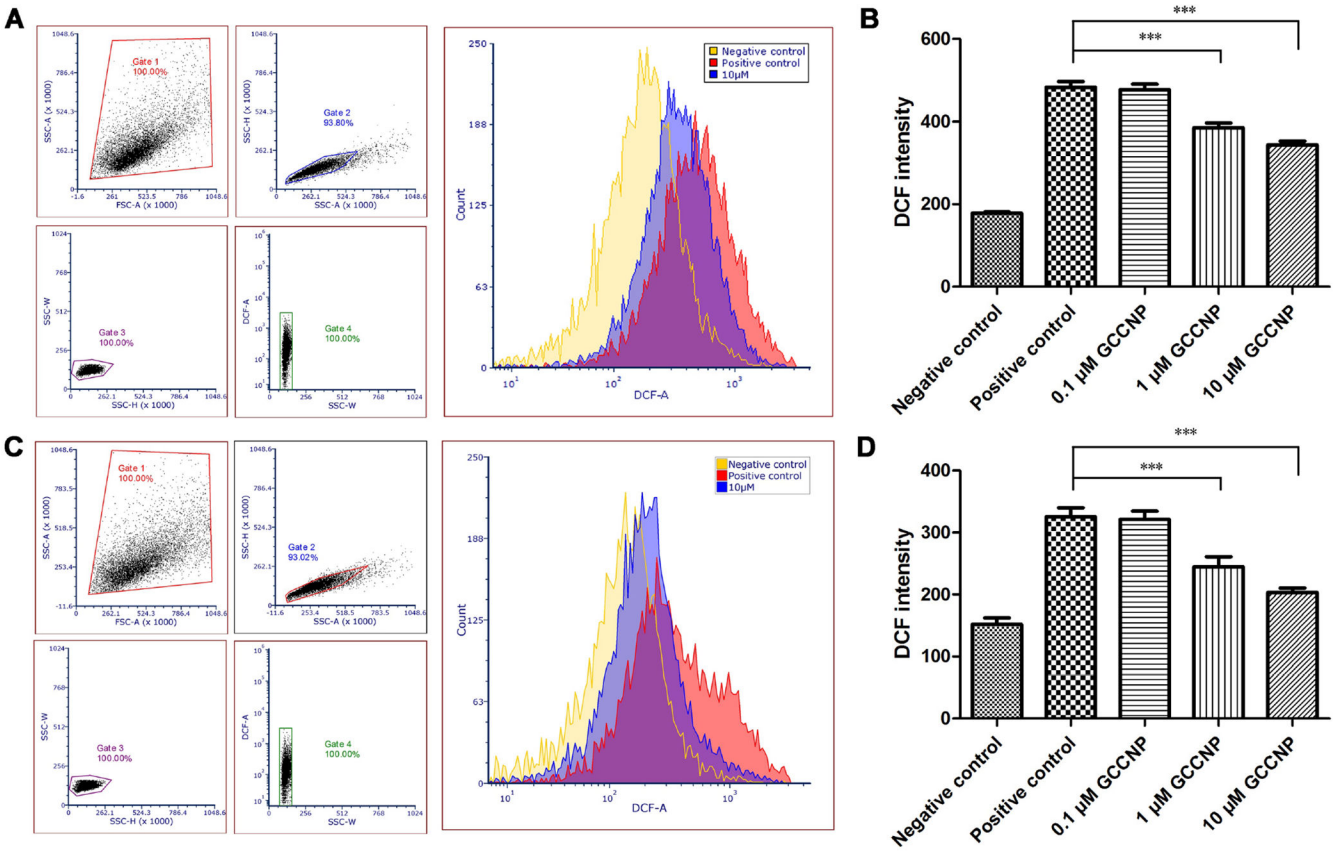

Figure 3. Detecting of ROS using DCF-DA.

Primary corneal cells (**A & B**) and conjunctival cells (**C & D**) were pre-treated with different concentration of GCCNP (0, 0.1, 1, and 10 μM) before exposure to H_2O_2 as described in the Methods. Total production of ROS was measured by DCF-DA assay. Left panels are representative of flow cytometry results from 10 μM GCCNP-treated primary corneal cells (**A**) and primary conjunctival cells (**C**); right panels are experimental results of DCF intensity in primary corneal cells (**B**) and primary conjunctival cells (**D**). For statistical analysis, treatments with compounds were compared to H_2O_2 (400 μM)-treated controls. Results are presented as means ± SEM from three parallel samples. * $p<0.05$, ** $p<0.01$, and *** $p<0.001$.

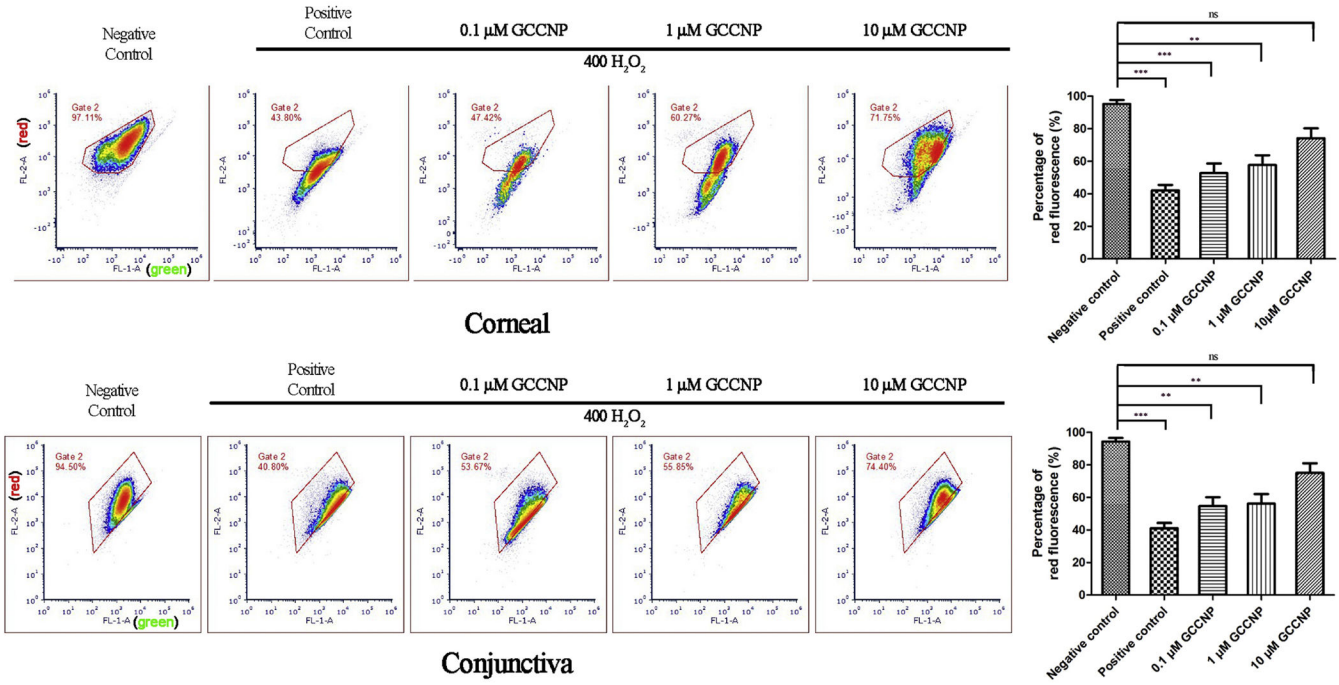

Figure 4. Recovery of H_2O_2-induced impairment of mitochondrial membrane potential through treatment with GCCNP.

(**A**) Corneal cell; (**B**) Conjunctiva cell. Results are presented as means ± SEM from three parallel samples. * $p<0.05$, ** $p<0.01$, and *** $p<0.001$.

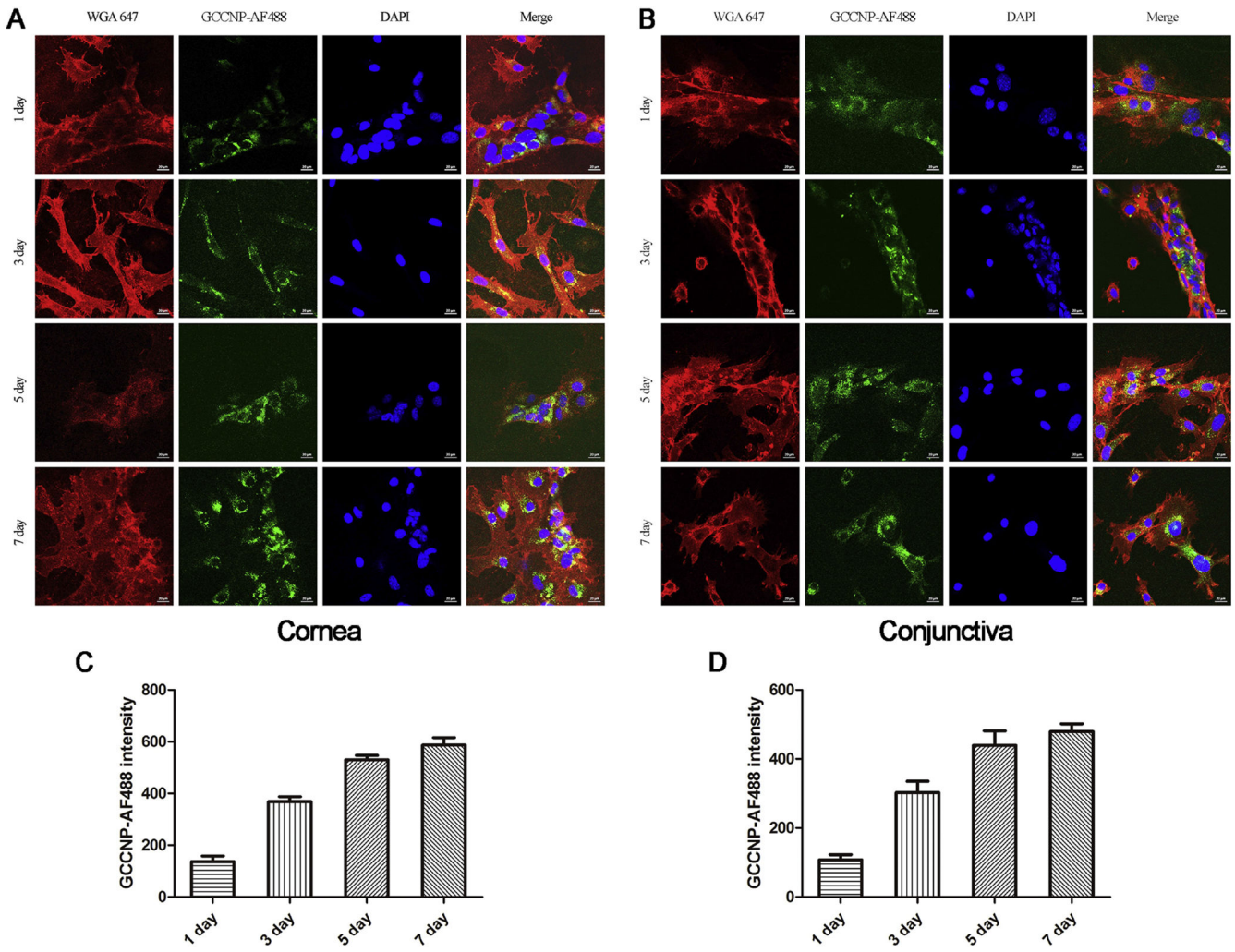

Figure 5. Cellular uptake of GCCNPs.

Representative images of primary corneal (**A**) and conjunctival (**B**) cells show the cellular uptake of AF488-labeled GCCNP. Quantitative flow cytometry data show corneal (**C**) and conjunctival (**D**) cells uptake AF488-labeled GCCNP at different time. Results are presented as means ± SEM from three parallel samples.

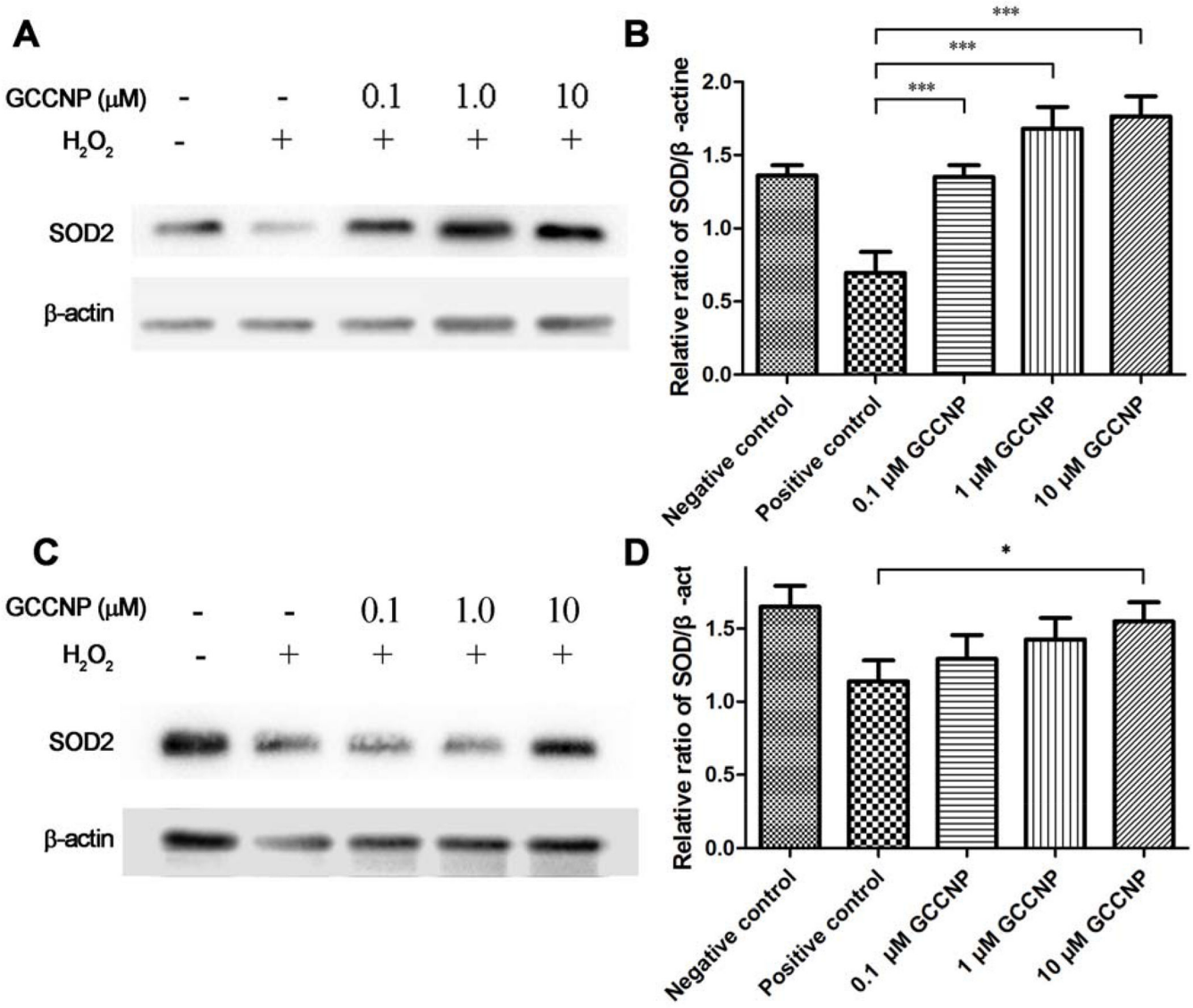

Figure 6. Western blot analysis the expression of SOD2.

Different concentration of GCCNP on the expression of SOD2 in the presence (positive control) or absence of H_2O_2 (negative control), and 0.1, 1.0 and 10μM GCCNP-treated groups in primary corneal cell (**A & B**) and conjunctival cell (**C & D**) were analyzed by Western blot. β-actin was used as an internal control. Representative data obtained from among three individual experiments. The graphs show the ratio of the signal intensities of SOD2/β-actin in primary corneal cell (**B**) and conjunctival cell (**D**). Results are presented as means ± SEM from three parallel samples. * $p<0.05$, ** $p<0.01$, and *** $p<0.001$.

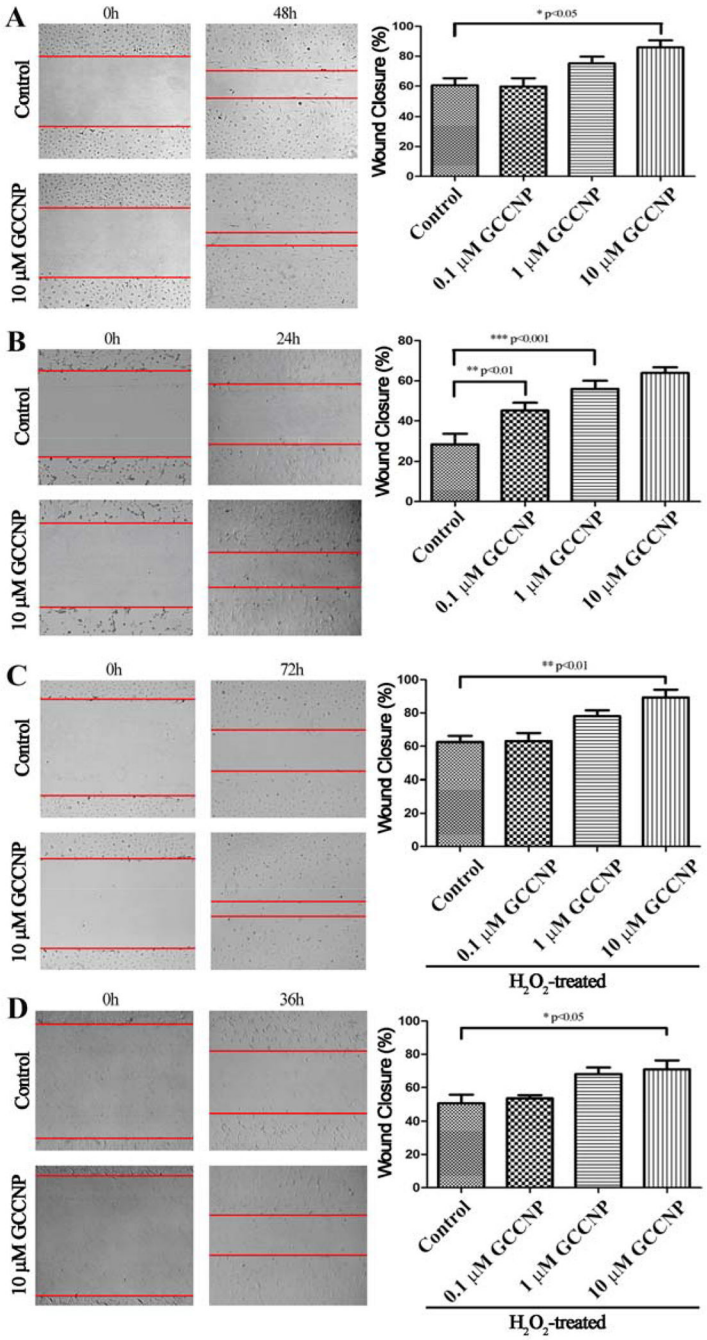

Figure 7. GCCNP promoted wound healing in primary corneal and conjunctival cells.

(**A**) Corneal cells. (**B**) Conjunctival cells. (*C*) 400 μM H_2O_2-treated corneal cells. (**D**) 400 μM H_2O_2-treated conjunctiva cells. Results are presented as means ± SEM from three parallel samples. * $p<0.05$, ** $p<0.01$, and *** $p<0.001$.

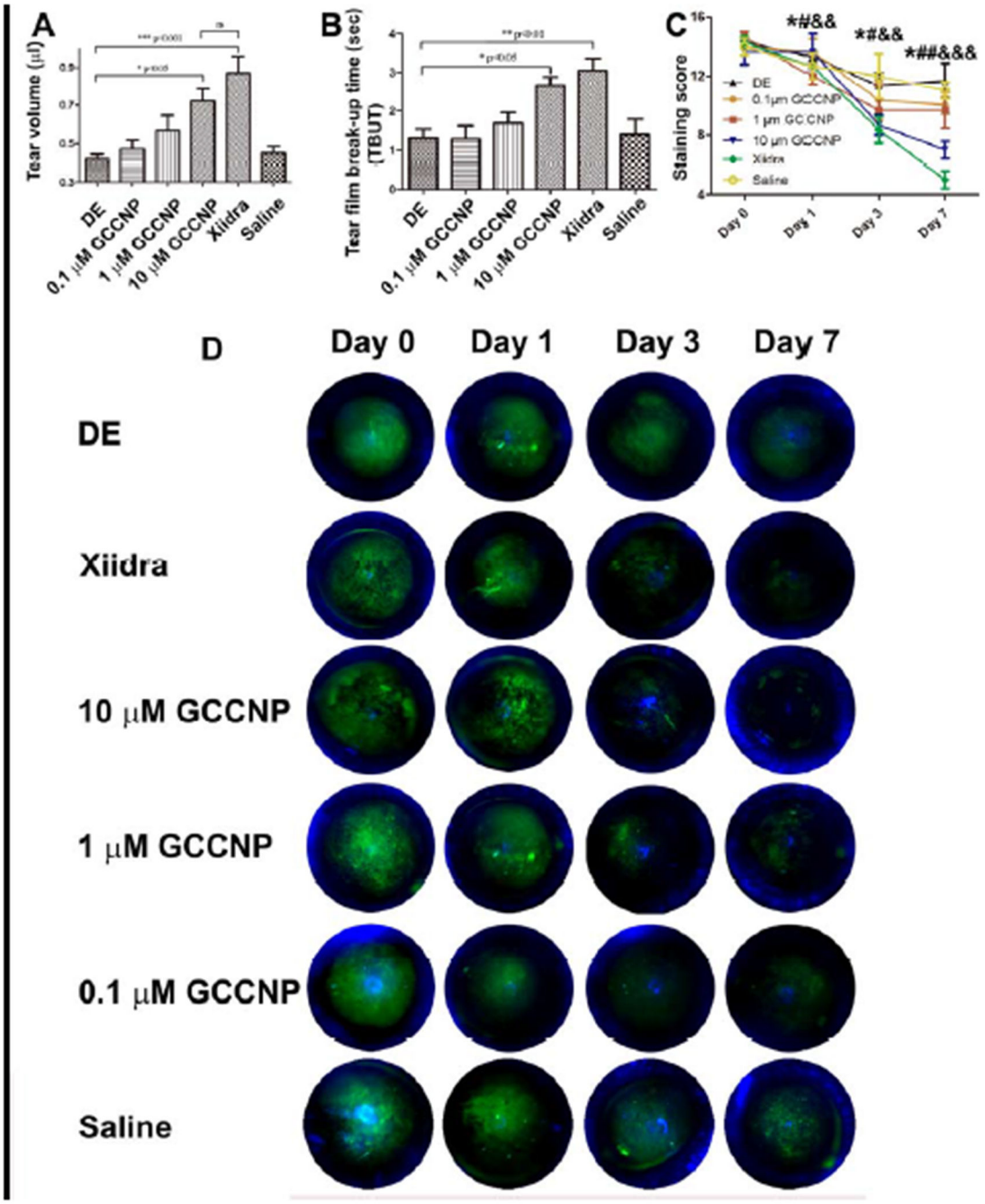

Figure 8.

(**A**) Mean tear volumes of the Dry eye, Xiidra, 0.1, 1 and 10 μM GCCNP-treated groups. (**B**) TBUT of the DE, GCCNP-treated groups and Xiidra-treated group. (**C**) Corneal fluorescein staining scores, and (**D**) Illustrations of the representative fluorescein staining images. Results are presented as means ± SEM from six parallel samples. *, #, or & $p<0.05$, **, ##, or && $p<0.01$, ***, ###, or &&& $p<0.001$, and ns $p>0.05$.

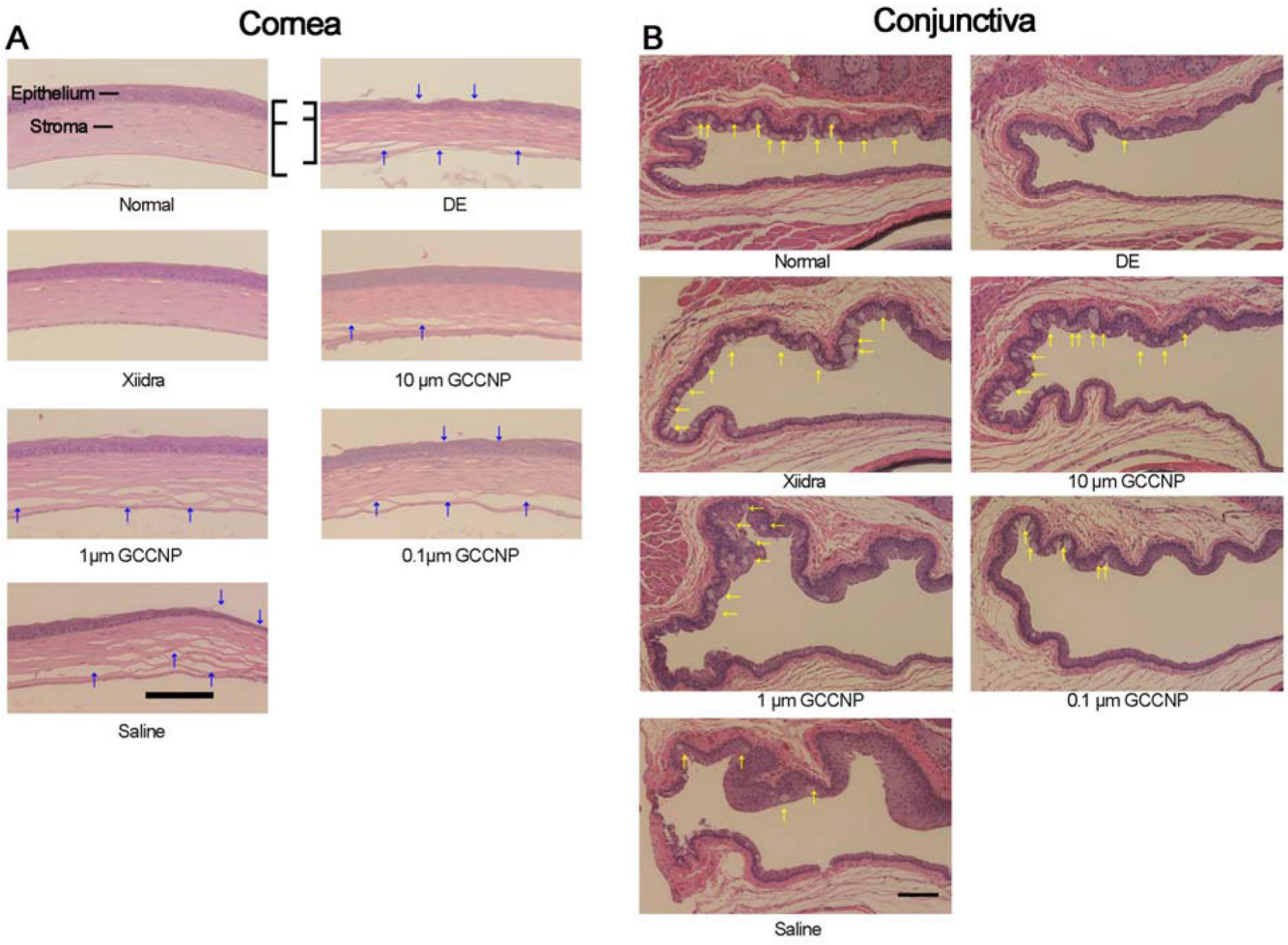

Figure 9.

Representative histological images of cornea and conjunctiva from normal mice, mice with dry eye, and after treatment with different concentration of GCCNP (10, 1, 0.1μM) for 7 days. (**A**) The corneal morphology is indicated by the blue arrows. (**B**) Goblet cells in the conjunctiva are indicated by the yellow arrows. The figure is a representative image from three independent experiments. Scale bar: 200 μm.

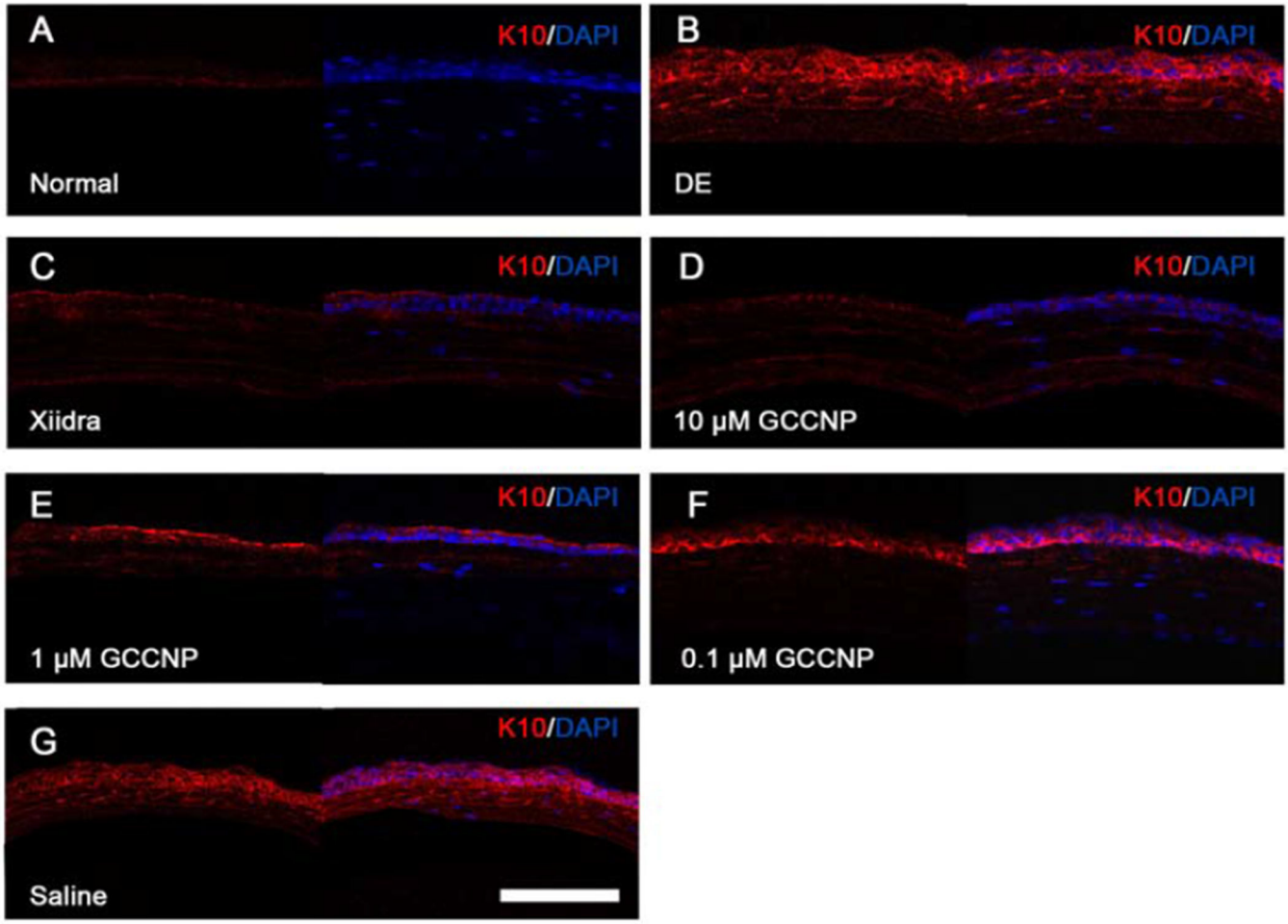

Figure 10. GCCNP ameliorated corneal epithelium squamous metaplasia.

The cryostat sections of normal, scopolamine hydrobromide -induced dry eye, and GCCNP treated dry eye corneas were stained with keratin 10 for corneal epithelium squamous metaplasia and cos-tained with DAPI for nuclear staining: (**A**) Normal cornea, (**B**) DE group, (**C**) Xiidra-treated, (**D**) 10μm GCCNP-treated, (**E**) 1μm GCCNP-treated, (**F**) 0.1μm GCCNP-treated, (**G**) Saline group. The left panels are K10 staining alone and right panels were the merged images of K10 and DAPI. The figure is the representative image of three independent experiments. Scale bar: 200 μm.